SOURCE IDENTIFICATION IN STRUCTURAL ACOUSTICS WITH AN INVERSE FREQUENCY RESPONSE FUNCTION TECHNIQUE

PROCEEDINGS OF ICNPAA-2002

R. Visser

Department of Mechanical Engineering – TMK
University of Twente
P.O. Box 217
7500 AE Enschede
The Netherlands
R.Visser@ctw.utwente.nl

ABSTRACT

Inverse source identification based on acoustic measurements is essential for the investigation and understanding of sound fields generated by structural vibrations of various devices and machinery.

Acoustic pressure measurements performed on a grid in the nearfield of a surface can be used to determine the vibration pattern of the surface at the frequency of interest. A general applicable method is the inverse frequency response function method (IFRF). The method is preferred, because it imposes no limitations on the shape of the measurement grid and the geometry of the source. Unfortunately, the inverse problem consists of solving an ill-conditioned system of equations, which can be only be performed by application of regularization (stabilization) techniques. Without these techniques the solution will be dominated by effects resulting from modeling errors and measurement noise.

The presentation investigates the physical nature of the ill-conditioned problem and explains how to deal with it. The quality of the approximated solution is mainly determined by the choice of a regularization parameter. This paper investigates the use of an L-curve plot for choosing the "optimal" parameter.

An illustration of the various steps in the acoustic source identification procedure will be given by means of a simulated experiment on the sound radiation of a rigid box covered by a flexible plate.

1. INTRODUCTION

Structural acoustics is focused on the relation between vibration patterns on the surface of a structure and the radiated sound field. The example in this paper concerns a rigid box covered by a simply supported flexible plate vibrating in a 2-1 mode with a frequency of 216.5 Hz, as shown in Figure 1. The box has the dimensions 0.15x0.2x0.4m. A set of 133 field points is used to measure the acoustic pressure in the free field at a distance of 0.06m from the source. The direct boundary element method (DBEM) is used to relate the normal velocities on the discretized geometry to the pressure in the set of field points. This relation is given by a frequency dependent, dense populated transfer matrix $\mathbf{H}$ (see [1]):

$$\mathbf{p}_{field} = \mathbf{H} \cdot \mathbf{v}_{normal} \tag{1}$$

Because the number of field points (133) exceeds the number of source nodes (125) in this example, the system is overdetermined.
When the velocity is prescribed (e.g. from a FEM calculation) and the transfer matrix is known (e.g. from a BEM calculation), the forward radiation problem of calculating the

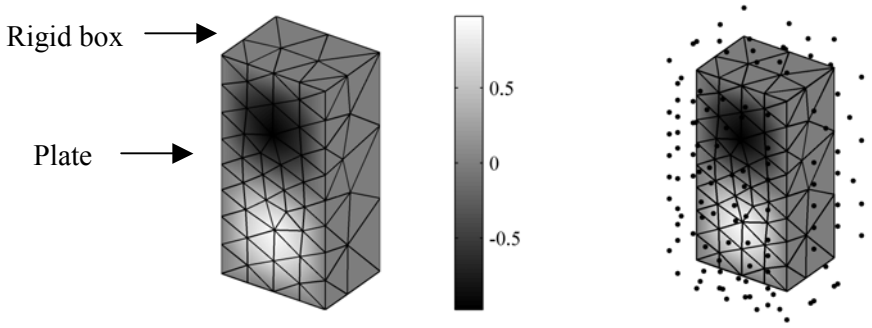

Figure 1: The normal velocity distribution of the example problem (left) and the discrete set of measurement points surrounding the box (right).

field pressures reduces to a simple matrix-vector multiplication.
However, in *inverse* acoustic source localization techniques, the task is to obtain the unknown surface velocities from the pressures measured at the field grid. Unfortunately, system (1) is a discrete ill-posed problem, which implies that arbitrary small perturbations in the measured pressure result in arbitrary large errors in the solution of the surface velocities. Therefore, solving the set of equations cannot be performed by standard least squares techniques.
In spite of the ill-conditioned nature of the problem, a meaningful solution can be found when regularization techniques are applied. This article explains the ill-conditioned nature in both physical and mathematical terms with the help of the numerical example of Figure 1.

2. DISCRETE ILL-POSED PROBLEMS

In regularization theory it is common to write the system of equations (1) as:

$$\mathbf{A}\mathbf{x} = \mathbf{b} \tag{2}$$

In inverse acoustics the challenge is to obtain a meaningful estimate of the original input of the system given by vector $\mathbf{x}$ (surface velocity). The complex data vector $\mathbf{b}$ is obtained from a pressure measurement and the transfer matrix $\mathbf{A}$ can be measured or calculated (BEM). As the matrix is ill-conditioned, standard inversion techniques fail to obtain a physically meaningful approximation of $\mathbf{x}$.
A superior numerical tool for analysis of discrete ill-posed problems is the singular value decomposition (SVD). The SVD reveals all the difficulties associated with the ill-conditioning of matrix $\mathbf{A}$.
Let $\mathbf{A} \in R^{m \times n}$ be a rectangular matrix with $m \geq n$. Then the SVD of matrix $\mathbf{A}$ is a decomposition of the form

$$\mathbf{A} = \mathbf{U}\Sigma\mathbf{V}^H = \sum_{i=1}^{n} \mathbf{u}_i \sigma_i \mathbf{v}_i^H \tag{3}$$

where $\mathbf{U} = (\mathbf{u}_1, \ldots, \mathbf{u}_m)$ and $\mathbf{V} = (\mathbf{v}_1, \ldots, \mathbf{v}_n)$ are unitary matrices, $\mathbf{U}^H\mathbf{U} = \mathbf{I}_m$; $\mathbf{V}\mathbf{V}^H = \mathbf{I}_n$, and where $\mathbf{\Sigma} = \mathrm{diag}(\sigma_1, \ldots, \sigma_n)$ has non-negative real diagonal elements appearing in descending order such that $\sigma_1 \geq \ldots \geq \sigma_n \geq 0$.

The numbers σ_i are the singular values of $\mathbf{A}$ while the vectors $\mathbf{u}_i$ and $\mathbf{v}_i$ are, respectively, the left and right singular vectors of $\mathbf{A}$. In connection with discrete ill-posed problems, two characteristic features of the SVD of $\mathbf{A}$ are often found [3,5]:

- The singular values σ_i decay gradually to zero with no particular gap in the spectrum.
- The left and right singular vectors $\mathbf{u}_i$ and $\mathbf{v}_i$ tend to have more sign changes in their elements as the index i increases, i.e., as σ_i decreases (vectors become more oscillatory).

Figure 2 clearly shows the gradual decay of singular values of the transfer matrix of our example problem from Figure 1.

2.1 Interpretation of SVD

Márki [2] showed that the singular vectors $\mathbf{u}_i$ and $\mathbf{v}_i$ can be interpreted as 'mode shapes' of the pressure on the field grid ($\mathbf{u}_i$) and normal velocity on the source surface ($\mathbf{v}_i$). The singular values couple each 'surface mode' of velocities independently to the corresponding 'field mode' of pressures. An important aspect of the SVD is that the singular vectors $\mathbf{u}_i$ and $\mathbf{v}_i$ become more oscillatory for higher indices i. In Figure 3, three source velocity modes are shown, the field modes are not shown because of the irregular field grid.

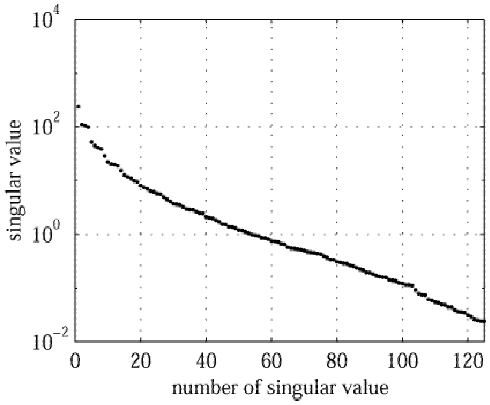

Figure 2: The singular values of the example problem clearly indicate the ill-conditioning of the problem.

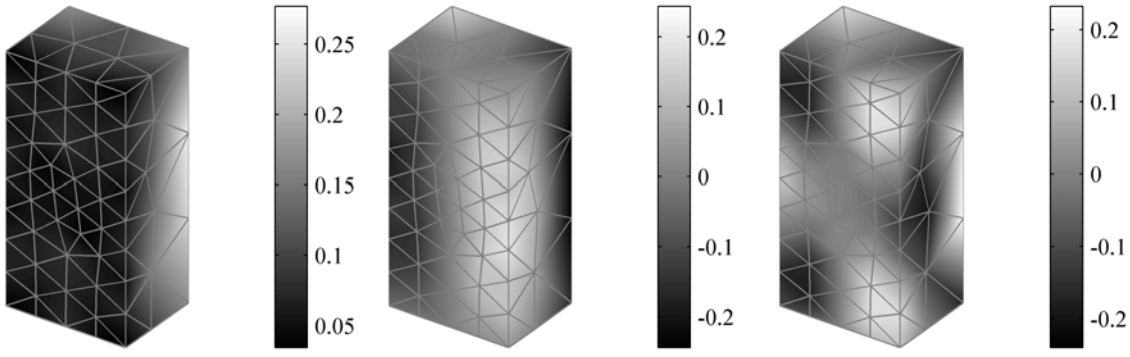

$\mathbf{v}_1; \sigma_1 = 235.0$ $\mathbf{v}_{10}; \sigma_{10} = 22.4$ $\mathbf{v}_{20}; \sigma_{20} = 8.06$

Figure 3: Smaller singular values have more oscillatory velocity modes (real-part).

3. DISCRETE PICARD CONDITION

We assume that the errors in the system of equations (2) mainly occur in the right-hand side $\mathbf{b}$. Thus the measured data $\mathbf{b}$ can be written as:

$$\mathbf{b} = \overline{\mathbf{b}} + \mathbf{e}, \qquad \overline{\mathbf{b}} = \mathbf{A}\overline{\mathbf{x}} \tag{4}$$

where $\overline{\mathbf{b}}$ represents the exact unperturbed data, $\overline{\mathbf{x}}$ represents the exact solution, and the vector $\mathbf{e}$ represents the errors in the data. These errors typically tend to have components in each left singular vector $\mathbf{u}_i$ (white noise in spatial sense).

In order to check the existence of a physically meaningful solution to the inverse problem and to ensure that this solution can be approximated by a regularized solution, it is necessary to satisfy the Discrete Picard Condition (DPC) [3]:

The exact SVD coefficients $\| \mathbf{u}_i^H \overline{\mathbf{b}} \|$ *decay faster than the singular values* σ_i.

Fulfillment of this condition assures that the exact, unknown, solution can be approximated by a regularized solution.

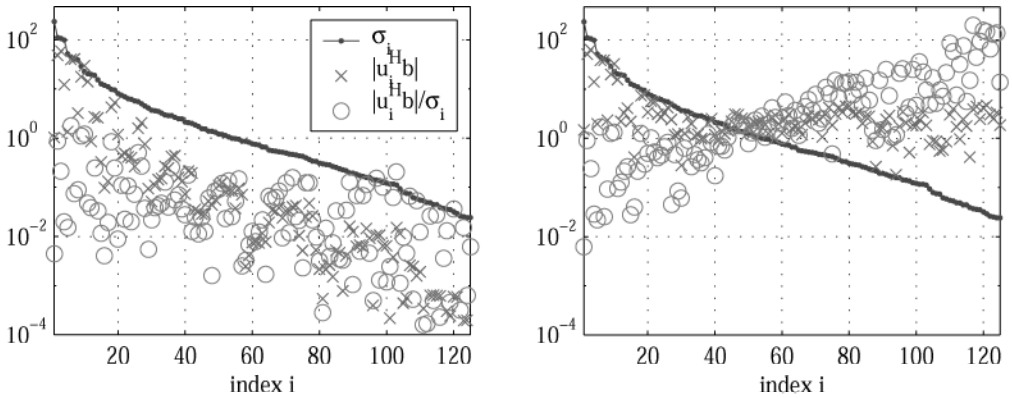

Figure 4: Picard plot for the unperturbed $\overline{\mathbf{b}}$ (left) and the perturbed $\mathbf{b}$ (right).

The left-hand part of Figure 4 gives the visualization of the DPC for the unperturbed data vector $\overline{\mathbf{b}}$. Obviously the 'average' decay of the SVD coefficients (crosses) is steeper than that of the singular values. This ensures that a meaningful regularized solution to our example problem can be obtained. The circles in the figure show the participation of each field mode to the solution. It can be seen that (some of) the first few modes will mainly determine the reconstructed velocity pattern and that there is no dominance of the higher modes.

The right-hand part of Figure 4 gives the Picard plot when the data vector $\mathbf{b}$ is contaminated with Gaussian noise at a S/N ratio of 20 dB. As the first few SVD coefficients fall off steeper than the singular values it is still possible to reconstruct a meaningful solution, but it can also be seen that the coefficients (crosses) level off at the noise level. The contributions to the solution (circles) show very clearly the dominant behavior of the higher modes with respect to the first few lower modes, which are important in the physically meaningful solution. This shows the disastrous influence of noise in ill-conditioned problems. The task of the regularization methods is to eliminate the influence of these higher modes in the solution.

4. REGULARIZATION OF THE SYSTEM OF EQUATIONS

If the SVD (3) is inserted in the system of equations (2) then it is straightforward to show that the standard least-squares solution $\mathbf{x}_{LS}$ becomes:

$$\mathbf{x}_{LS} = \mathbf{V}\boldsymbol{\Sigma}^{-1}\mathbf{U}^H = \sum_{i=1}^{n} \frac{\mathbf{u}_i^H \mathbf{b}}{\sigma_i}\mathbf{v}_i = \sum_{i=1}^{n}\left(\frac{\mathbf{u}_i^H \overline{\mathbf{b}}}{\sigma_i}\mathbf{v}_i + \frac{\mathbf{u}_i^H \mathbf{e}}{\sigma_i}\mathbf{v}_i \right) \tag{5}$$

For well-posed problems this gives accurate predictions of solution $\mathbf{x}$. For ill-conditioned problems the first term between brackets (5) satisfies the DPC and thus decreases for smaller singular values. Unfortunately, the error term does not satisfy the DPC and will grow rapidly for smaller singular values and eventually will dominate the solution (see right-hand side plot in Figure 4). As a consequence, the least-squares solution (5) has many sign changes due to the oscillatory nature of the higher modes $\mathbf{u}_i$ and $\mathbf{v}_i$ and appears completely random (see Figure 7).

With this knowledge it is easy to understand that the purpose of a regularization method is to damp or filter out the contributions to the solution corresponding to the small singular values. Hence, a regularized solution $\mathbf{x}_{reg}$ is sought in the form of:

$$\mathbf{x}_{reg} = \sum_{i=1}^{n} f_i \frac{\mathbf{u}_i^H \mathbf{b}}{\sigma_i}\mathbf{v}_i \tag{6}$$

Here, f_i are the filter factors for the particular regularization method. The filter factors must have the important property that for decreasing σ_i, the corresponding f_i tends to zero in such a way that the contributions $(\| \mathbf{u}_i^H \mathbf{b} \| / \sigma_i)\mathbf{v}_i$ to the solution from the smaller σ_i are filtered out. The difference between the various regularization methods lies essentially in the way in which these filter factors are defined. Hence, the filter factors play an important role in connection with regularization theory, and it is worthwhile to characterize the filter factors for the regularization methods that are used in this paper.

4.1 Truncated Singular Value Decomposition - TSVD

The most commonly applied method is the truncated SVD, which simply truncates the number of singular values which is considered in the solution $\mathbf{x}_{reg}$

$$\mathbf{x}_{reg} = \sum_{i=1}^{n} f_i \frac{\mathbf{u}_i^H \mathbf{b}}{\sigma_i}\mathbf{v}_i \text{ with } f_i = 1 \ \forall \ i \in [1,k] \text{ and } f_i = 0 \ \forall \ i \in [k+1,n] \tag{7}$$

The TSVD eliminates the influence of all singular vectors associated with singular values above σ_k. The parameter k is called the regularization parameter which determines the amount of filtering (or regularization) applied to the least-squares solution. How to choose the optimal truncation parameter will be discussed in the section on the L-curve criterion.

4.2 Damped Singular Value Decomposition - DSVD

A less known regularization method is the damped SVD. Here, instead of using filter factors 0 and 1 as in TSVD, a smoother cut-off is defined

$$f_i = \frac{\sigma_i}{\sigma_i + \lambda} \quad \forall i \in [1, n] \tag{8}$$

where λ is an arbitrary chosen parameter. These filter factors have only a slight influence on the high singular values but suppress the smaller singular values which are responsible for the ill-conditioned behaviour of the solution. How to efficiently choose the regularization parameter λ will be discussed also in the section on the L-curve.

4.3 Tikhonov

Besides TSVD, Tikhonov regularization plays a central role in regularization theory. For Tikhonov regularization the filter factors are defined by

$$f_i = \frac{\sigma_i^2}{\sigma_i^2 + \lambda^2} \quad \forall i \in [1, n] \tag{9}$$

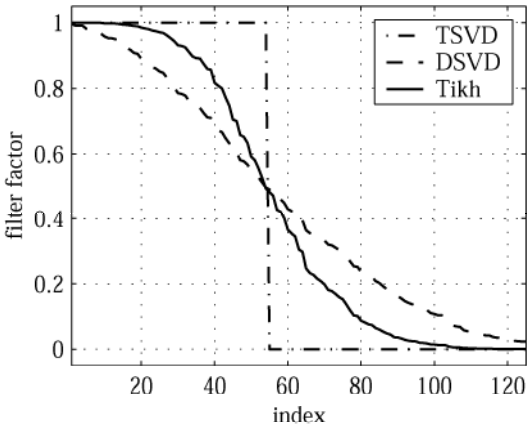

Figure 5: Filter factors for the three regularization methods

These filter factors decay faster than the DSVD filter factors and effective filtering is obtained for singular values $\sigma_i < \lambda$.

In Figure 5 the filter factors for the different regularization methods are shown.

Evidently all regularization methods act as low-pass filters in the singular value spectrum. They effectively filter out the small singular values, which are responsible for the dominance of the highly oscillatory modes in the reconstructed velocity pattern.

5. L-CURVE CRITERION

Perhaps the most convenient graphical tool for the selection of the optimal regularization parameters is the so-called L-curve, which is a plot of the norm $\eta = \| \mathbf{x}_{reg} \|_2$ of the regularized solution versus the corresponding residual norm $\rho = \| \mathbf{A}\mathbf{x}_{reg} - \mathbf{b} \|_2$. The L-curve clearly visualizes the compromise between minimalization of these two quantities, which is essential in any regularization method [4,5,6].

When the L-curve is plotted in a log-log scale, almost always a characteristic L-shaped curve appears (hence its name) with a distinct corner separating the vertical and horizontal parts of the curve. Both regions can be explained from two error types in the regularized solution

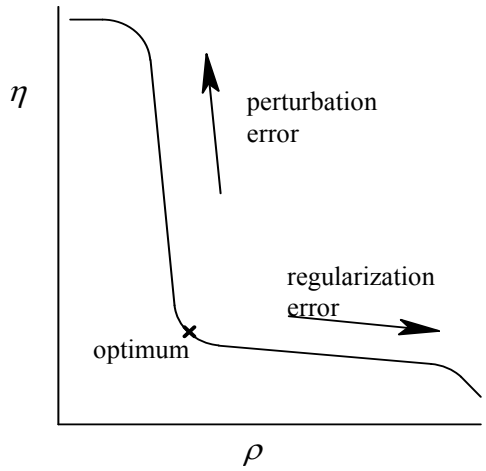

$$\mathbf{x}_{reg} - \overline{\mathbf{x}} = \sum_{i=1}^{n}\left(f_i \frac{\mathbf{u}_i^H \overline{\mathbf{b}}}{\sigma_i}\mathbf{v}_i + f_i \frac{\mathbf{u}_i^H \mathbf{e}}{\sigma_i}\mathbf{v}_i \right) - \sum_{i=1}^{n} \frac{\mathbf{u}_i^H \overline{\mathbf{b}}}{\sigma_i}\mathbf{v}_i$$
$$= \sum_{i=1}^{n}(f_i - 1)\frac{\mathbf{u}_i^H \overline{\mathbf{b}}}{\sigma_i}\mathbf{v}_i + \sum_{i=1}^{n} f_i \frac{\mathbf{u}_i^H \mathbf{e}}{\sigma_i}\mathbf{v}_i \qquad (10)$$

The error given by the first summation in (10) is solely caused by the regularization method and is called the *regularization error*. The error given by the second summation finds its origin in the errors of the data vector $\mathbf{b}$ and is called the *perturbation error*.
The horizontal part of the L-curve corresponds to solutions in which the regularization error dominates (e.g. too much filtering). In contrast, the vertical part of the L-curve corresponds to solutions dominated by the perturbation error (too less filtering).
The optimal regularization parameter is found in the corner of the L-curve. The DSVD performs unsatisfactory, the corner of its L-curve is less distinct than for the other two methods and the solutions tend to be of lower quality. There seems to be little difference between the Tikhonov solution and the TSVD solution. However, the first gives usually

slightly better L-shaped curves. As the reconstructed velocity patterns of the two methods are comparable, only the reconstructions with the Tikhonov regularization will be shown.

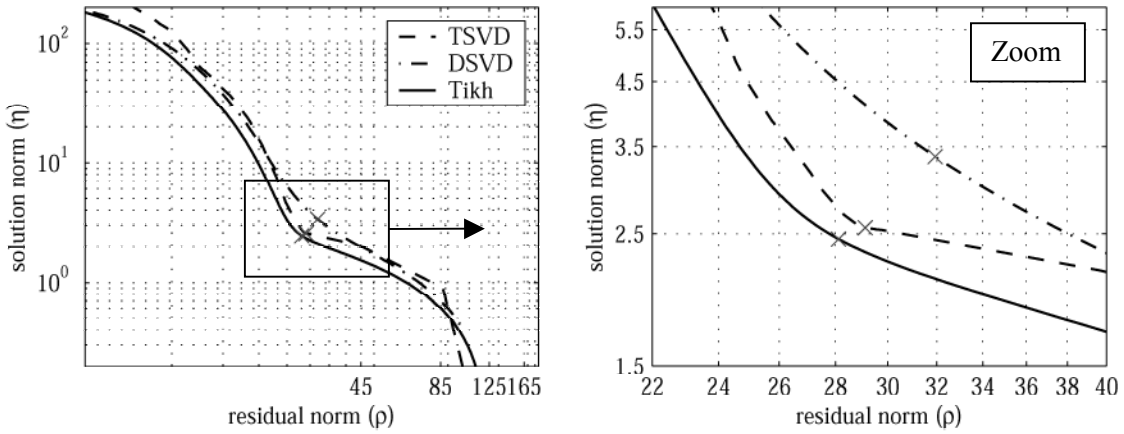

Figure 6: L-curve plots for the 3 regularization methods ('x' indicates optimum).

6. RECONSTRUCTED VELOCITY DISTRIBUTIONS

Figure 7 shows the reconstructed result from a 'numerical' pressure measurement, which has been artificially contaminated with noise. In the first picture the regularization parameter λ was chosen too low resulting in too less filtering. Therefore the perturbation error associated with the highly oscillatory modes $\mathbf{v}_i$ is dominant in the reconstructed results. The large amplitude indicates the division of errors by small singular values. For the middle picture the regularization parameter was selected by the L-curve criterion (see Figure 6). This shows a very good reconstruction of the original prescribed 2-1 vibration mode as given in Figure 1. Finally the last picture was created with too much regularization and thus results in a too smooth velocity distribution. The excessive filtering causes severe decay in the amplitude of the reconstruction.

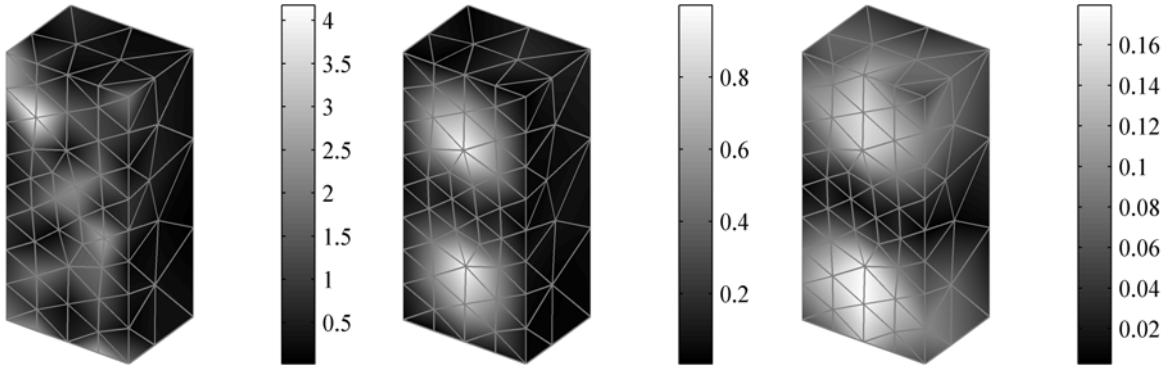

Figure 7: Reconstructed velocity amplitudes using Tikhonov regularization with 3 different parameters and a S/N-ratio of 20 dB.

CONCLUSIONS

This paper discussed three regularization methods for nearfield acoustic source identification problems. By means of a numerical example, it was shown that the choice of a correct regularization parameter is vital for the quality of the reconstructed velocity field. The L-curve criterion results in an easy understandable and robust graphical method for choosing this optimal regularization parameter.

For the numerical example presented in this paper, it was shown that both TSVD and Tikhonov regularization are well suited to be used in combination with the L-curve criterion whereas the DSVD method proved to be less suitable for solving this inverse acoustic problem.

ACKNOWLEDGEMENTS

This research is supported by the Dutch Technology Foundation (STW).

REFERENCES

1. R.D. Ciskowski, C.A. Brebbia, *Boundary Element Methods in Acoustics*, (Computational Mechanics publications, 1991)
2. F. Márki, F. Augusztinovicz, “Effects, interpretation and practical application of truncated SVD in the numerical solution of inverse radiation problems”, Proceedings ISMA25 Leuven, 1405-1413 (2000)
3. P.C. Hansen, “The discrete Picard condition for discrete ill-posed problems”, BIT, **30**, 658-672 (1990)
4. C.L. Lawson, R.J. Hanson, *Solving least squares problems*, (Prentice-Hall, Englewood Cliffs, 1974)
5. P.C. Hansen, “Regularization tools: A Matlab package for analysis and solution of discrete ill-posed problems”, Numerical Algorithms, **6**, 1-35 (1994)
6. P.C. Hansen, O'Leary, “The use of the L-curve in the regularization of discrete ill-posed problems”, SIAM Journal of Scientific Computing, **14**, 1487-1503 (1993)